



## UvA-DARE (Digital Academic Repository)

### Self-assembly of colloidal cube superstructures with critical Casimir attractions

Kennedy, C.L.; Sayasilpi, D.; Schall, P.; Meijer, J.M.

**DOI**

[10.1088/1361-648X/ac5866](https://doi.org/10.1088/1361-648X/ac5866)

**Publication date**

2022

**Document Version**

Final published version

**Published in**

Journal of Physics Condensed Matter

**License**

CC BY

[Link to publication](#)

**Citation for published version (APA):**

Kennedy, C. L., Sayasilpi, D., Schall, P., & Meijer, J. M. (2022). Self-assembly of colloidal cube superstructures with critical Casimir attractions. *Journal of Physics Condensed Matter*, 34(21), [214005]. <https://doi.org/10.1088/1361-648X/ac5866>

**General rights**

It is not permitted to download or to forward/distribute the text or part of it without the consent of the author(s) and/or copyright holder(s), other than for strictly personal, individual use, unless the work is under an open content license (like Creative Commons).

**Disclaimer/Complaints regulations**

If you believe that digital publication of certain material infringes any of your rights or (privacy) interests, please let the Library know, stating your reasons. In case of a legitimate complaint, the Library will make the material inaccessible and/or remove it from the website. Please Ask the Library: <https://uba.uva.nl/en/contact>, or a letter to: Library of the University of Amsterdam, Secretariat, Singel 425, 1012 WP Amsterdam, The Netherlands. You will be contacted as soon as possible.

PAPER • OPEN ACCESS

## Self-assembly of colloidal cube superstructures with critical Casimir attractions

To cite this article: Chris L Kennedy *et al* 2022 *J. Phys.: Condens. Matter* **34** 214005

View the [article online](#) for updates and enhancements.

You may also like

- [Dynamics and steady states of a tracer particle in a confined critical fluid](#)  
Markus Gross
- [Fluctuation induced forces in critical films with disorder at their surfaces](#)  
A Macioek, O Vasilyev, V Dotsenko et al.
- [The square lattice Ising model on the rectangle III: Hankel and Toeplitz determinants](#)  
Alfred Hucht

# Self-assembly of colloidal cube superstructures with critical Casimir attractions

Chris L Kennedy<sup>1,2</sup> , Daphne Sayasilpi<sup>3</sup>, Peter Schall<sup>3</sup>  
and Janne-Mieke Meijer<sup>1,2,\*</sup> 

<sup>1</sup> Department of Applied Physics, Eindhoven University of Technology, Groene Loper 19, 5600 MB Eindhoven, The Netherlands

<sup>2</sup> Institute for Complex Molecular Systems, Eindhoven University of Technology, PO Box 513, 5600 MB Eindhoven, The Netherlands

<sup>3</sup> Institute of Physics, University of Amsterdam, Science Park 904, 1098 XH Amsterdam, The Netherlands

E-mail: [j.m.meijer@tue.nl](mailto:j.m.meijer@tue.nl)

Received 15 December 2021, revised 15 February 2022

Accepted for publication 24 February 2022

Published 21 March 2022



CrossMark

## Abstract

The structure of self-assembled materials is determined by the shape and interactions of the building blocks. Here, we investigate the self-assembly of colloidal ‘superballs’, i.e. cubes with rounded corners, by temperature-tunable critical Casimir forces to obtain insight into the coupling of a cubic shape and short range attractions. The critical Casimir force is a completely reversible and controllable attraction that arises in a near-critical solvent mixture. Using confocal microscopy and particle tracking, we follow the self-assembly dynamics and structural transition in a quasi-2D system. At low attraction, we observe the formation of small clusters with square symmetry. When the attraction is increased, a transition to a rhombic  $\Lambda_1$ -lattice is observed. We explain our findings by the change in contact area at faces and corners of the building blocks combined with the increase in attraction strength and range of the critical Casimir force. Our results show that the coupling between the rounded cubic shape and short-range attraction plays a crucial role for the superstructures that form and provide new insights for the active assembly control of micro and nanocubes.

Keywords: superballs, phase transitions, anisotropic colloids, colloidal crystals, critical Casimir force

 Supplementary material for this article is available [online](#)


(Some figures may appear in colour only in the online journal)

## 1. Introduction

The shape of colloidal particles influences their phase behaviour and the superstructures they can assemble into.

While spheres will form fluid and crystal phases [1], colloidal rods and platelets will form liquid crystal phases including nematic, smectic and columnar phases [2–4]. Today, thanks to advances in synthesis, colloidal particles are available in an abundance of different shapes [5, 6], including colloidal molecules [7] and faceted shapes, such as cubes [8], tetrahedra [9, 10], dodecahedra [11] and icosahedra [12]. Inspired by these anisotropic shapes, extensive simulation studies have shown for various polyhedral shapes that, driven by shape and excluded volume interactions alone, these particles will assem-

\* Author to whom any correspondence should be addressed.

 Original content from this work may be used under the terms of the [Creative Commons Attribution 4.0 licence](#). Any further distribution of this work must maintain attribution to the author(s) and the title of the work, journal citation and DOI.

ble into a diversity of phases including liquid crystals, plastic crystals and crystals [13, 14]. A main driving force for the formation of the different phases is the alignment of the flat facets/faces of the particles.

The superstructures formed by anisotropic particles are also very sensitive to the exact interparticle interactions present during the assembly. Experimentally, short-range attractive interactions can be induced between the particles via hydrophobic interactions [15], depletion forces [16, 17], DNA brushes [18, 19], solvent evaporation [20], or critical Casimir forces [21]. For faceted nanoparticles assembled via DNA brushes many different superlattices can be achieved due to the specific interactions between the facets [18, 22]. Interestingly, for nanocubes interacting via different attractive interactions, the formation of a variety of different superstructures switching from simple cubic via rhombic to face-centred cubic crystals [23], and even body-centred tetragonal lattices [20, 24] have been observed. Also for micron sized particles, although available in less versatile shapes, attractive forces have been shown to induce different phase behaviour and superstructures [25]. For instance, different liquid crystal phases and glasses have been found for platelets [26] and rods [27] as well as fiber-like assemblies for disks [28] and ellipsoids [29]. Interestingly, also for micron-sized cubes interacting via depletion attractions the formation of simple cubic, rhombic and face-centred crystals has been observed [8, 30–32]. However, while the combination of faceted anisotropic shapes and attractive interactions clearly influences the superstructure symmetry, the coupling between the two is not yet fully understood.

Recently, critical Casimir forces have been employed as a controllable method to directly tune short-range attractions between colloids *in situ* [21, 33]. Critical Casimir forces take advantage of solvent mediated interactions in near-critical solvents. The attractive interactions arise from the confinement of temperature dependent solvent concentration fluctuations between the particle surfaces [34, 35] and allow the attractive potential between the colloids to be tuned [36]. In this way the formation of liquid phases and crystals of colloidal spheres has been investigated [37, 38]. So far, this temperature-driven assembly has been also successfully employed for spherical particles with anisotropic patchy interactions [39–42]. These studies revealed the switching of interacting Janus particles sides [39], while particles interacting with two and more patches were shown to lead to the formation of colloidal polymers [40] and colloidal molecules [41]. In addition, the assembly of nanoparticles on an surface was shown to allow tuning of disordered or ordered structures [42].

Here, we apply the critical Casimir force to the assembly of shape-anisotropic cubic colloids. We show that the tuning of short-range attraction leads to switching between two distinct superstructures. At low attraction bonding occurs between the cube faces leading to directional interactions and the formation of dense clusters with square symmetry. We show that for these anisotropic particles *in situ* control over the bond energy between the particles can be achieved. At high attraction close to the solvent critical point the dense clusters show a structural

transition from square to rhombic  $\Lambda_1$ , which is similar to the different structures and transitions often observed in nanocube assemblies [20, 23, 24]. In the current case, we argue that a subtle change surface contact area caused by the combination of increasing attraction range and finite details of the cubic particle shape, with facets and rounded corners, is responsible for the structural transition. Our results show that there is a fine coupling between the particle shape and attractive interaction, and that their combination leads to different directional interactions and superstructures. In addition, our experiments open new routes to investigate the self-assembly processes of faceted anisotropic building blocks *in situ* and to gain insight into the important role the coupling of short-range attraction and finite shape details play for the final superstructure symmetry.

## 2. Materials and methods

### 2.1. Particle dispersion preparation

Hollow silica cubes labeled with an inner rhodamine shell and non-labeled outer shell were synthesised via well established literature protocols for silica coated hematite cubes, followed by dissolution of the iron oxide cores [8, 30, 43]. This synthesis yields particles with a shape well approximated by a superball:

$$\left|\frac{x}{a}\right|^m + \left|\frac{y}{a}\right|^m + \left|\frac{z}{a}\right|^m \leq 1, \quad (1)$$

where  $m$  is the shape parameter which ranges from 2 (sphere) to  $\infty$  (cube) and  $a = L/2$  with  $L$  the edge length as shown in figure 1(b). Particle measurements were made on transmission electron micrographs such as that shown in figure 1(a). The mean  $L$  was found to be  $1.40 \mu\text{m}$ , with polydispersity,  $\delta_L = 5\%$  and  $m = 2.9$ . For further details see supplementary section 1 and figure S1 (<https://stacks.iop.org/JPCM/34/214005/mmedia>).

A mixture containing 28.40 wt% 2,6-lutidine ( $\geq 99\%$ , Sigma-Aldrich) in deionised water ( $18.2 \text{ M}\Omega \text{ cm}$ , Merck Millipore) was employed. This mixture is slightly lutidine rich compared to the critical composition of 28 wt% lutidine to induce critical Casimir interactions between hydrophilic silica particles [44, 45]. The silica cubes were dispersed into this mixture via centrifugation ( $200 \mu\text{l}$  dispersion centrifuged  $3 \times$  at  $1000 \text{ g}$  for  $5 \text{ min}$ ) and the final concentration was adjusted to  $0.25 \text{ vol}\%$ . All liquid handling after particle introduction was done with plastic pipette tips which were rinsed twice with deionised water and once with the lutidine/water mixture before use, to remove any impurities. Dispersions were prepared and imaged on the same day, as the behaviour of silica particles dispersed in lutidine mixtures is known to change over time [46].

### 2.2. Temperature controlled confocal microscopy

The colloidal cube dispersion was imaged in a rectangular capillary (borosilicate,  $0.2 \times 2 \times 50 \text{ mm}$ , Vitrocom) that was pretreated with alkaline cleaner (Hellmanex III,  $100 \times$  diluted) to increase hydrophilicity of the glass and remove impurities. The

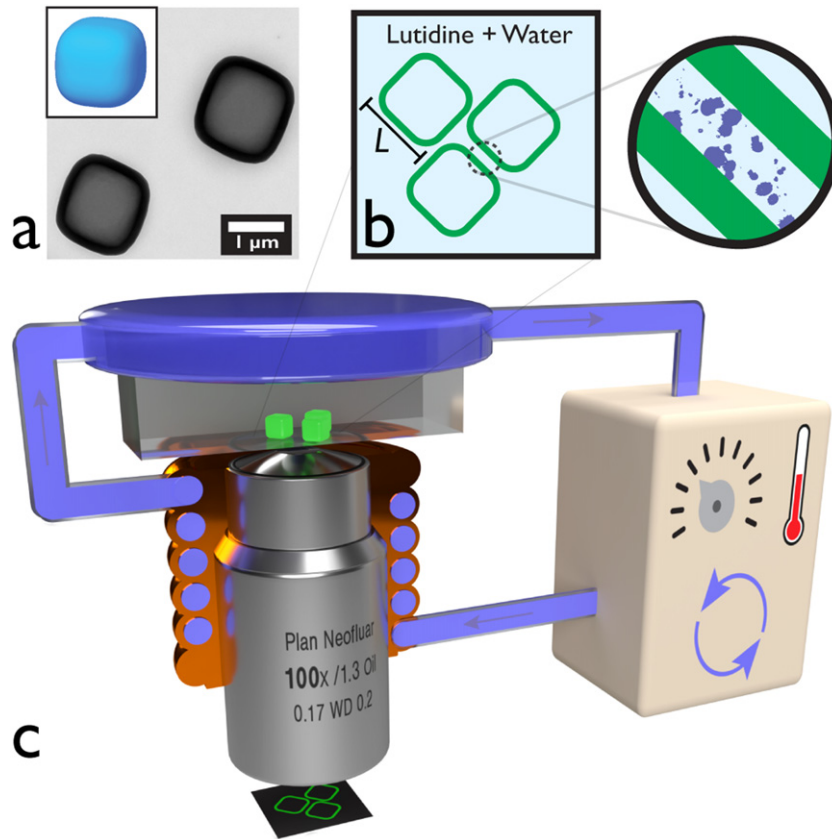


**Figure 1.** Overview of the experimental setup. (a) Transmission electron micrograph of the cubic colloids. Inset shows a 3D rendering of the superball shape of the particles. (b) Sketch depicting cubes in the binary solvent mixture. Magnified view shows representation of the critical fluctuations confined between the particle surfaces which result in the critical Casimir force. (c) Schematic representation of microscopy setup used for imaging cubic particles on the bottom surface of sample capillary (not to scale). Temperature control was provided by water circulation from a water bath (right) through an objective collar (shown in cross-section) and stage-mounted chamber (top).

capillary cell was prepared by first sealing one end with fluorocarbon grease (Krytox LVP), followed by filling the capillary from the other end with  $18 \mu\text{l}$  of the particle dispersion using a pipette and finally sealing with the same grease.

The confocal microscopy setup including a custom built temperature control system is depicted in figure 1(c). The capillary was mounted on the underside of a glass chamber through which water of controlled temperature was pumped by a circulating bath (Julabo F25 ME). Part of the same water flow circuit was a metal collar around the objective. In this way, the glass chamber, objective lens, immersion oil and sample capillary all have the temperature specified by the thermostat in the water bath (with a precision of  $\pm 0.02 \text{ }^\circ\text{C}$ ) [47]. Images were obtained using a confocal laser scanning microscope (CLSM, Zeiss LSM5 Live) equipped with a  $100\times/1.3$  oil immersion objective and a 532 nm laser for excitation of the rhodamine dye. Series of 2D images were captured of a  $67 \times 67 \mu\text{m}$  field of view with a  $1024 \times 1024$  pixel raster and a time step of  $t = 1.5 \text{ s}$  between frames. Measurements were performed at different temperatures with different equilibration times. At the highest temperatures (strongest attraction), particles were seen to more often stick to the glass and disrupt the assembly behaviour. To minimize the time available for particle sticking, the temperature was raised rapidly when probing the strong attraction regime.

After collecting data, the sample was further heated while imaging to observe the temperature of solvent phase separation,  $T_{\text{cx}}$ . This is not the critical temperature,  $T_c$ , because the mixture did not have the critical composition, but a slightly lower lutidine fraction, ‘ $x$ ’. As  $T_{\text{cx}}$  is very sensitive to experimental details, the exact value needs to be determined *in situ* and all temperatures reported as  $\Delta T = T_{\text{cx}} - T$  [35].

### 2.3. Image analysis

Particle centre coordinates were extracted from each frame using Trackpy [48] on the blobs resulting from a single-radius circle Hough transform. Particles with centres closer than  $1.3D$  ( $1.76 \mu\text{m}$ ) were identified as nearest neighbours (NNs). The neighbours of each particle were used to compute the 2D bond order parameters:

$$\psi_k = \langle \exp^{ik\theta_j} \rangle_{j \in \text{NN}}, \quad (2)$$

where  $k \in \{4, 6\}$ , the average is over a particle’s NNs and  $\theta_j$  is the polar angle of the bond connecting the centres of particle and neighbour.  $\psi_4$  and  $\psi_6$  were used to classify the crystal environment of each particle with at least two neighbours. Particles with  $\psi_4 > 0.85$  were assigned ‘square’ and those with  $\psi_6 > 0.85$  were assigned  $\Lambda_1$ , which is a distorted hexagonal phase [49]. Particles with  $\psi_4$  and  $\psi_6$  both less than

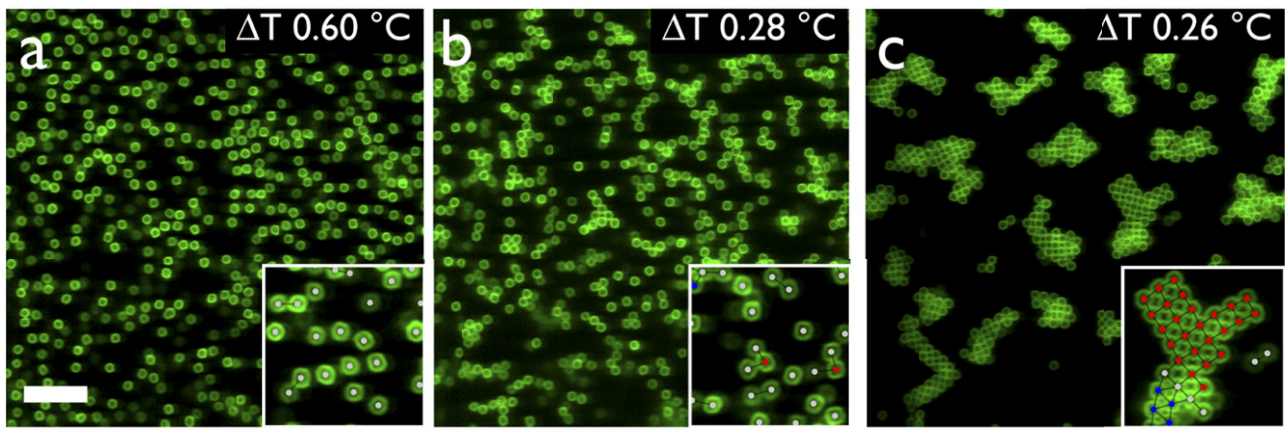


**Figure 2.** CLSM snapshots showing clustering of cubic silica particles induced by critical Casimir forces at increasing temperature. With increasing temperature the system changes from (a) an isotropic fluid phase, via (b) a fluid with the formation of small transient clusters to (c) a system with large stable particle clusters. Insets show magnified views with detected particle centres as dots and identified NNs connected by lines. The colours indicate assigned particle environments: square (red),  $\Lambda_1$  (blue) and unassigned (grey). The scale bar in (a) has length  $10 \mu\text{m}$  and the inset windows have side length  $13 \mu\text{m}$ .

or both greater than 0.85 were not assigned. Particles in linear branches (two neighbours and bond angle  $<20^\circ$ ) were also not assigned because their environment cannot meaningfully be described as either square or ‘hexagonal’.

#### 2.4. Surface contact calculation

To make predictions about the lowest energy configuration of the particles in quasi-2D, an approximate model was used. This model used superdisks (2D equivalent of superballs, defined by equation (1) with  $z = 0$ ) with  $m = 2.9$  and  $a = 700 \text{ nm}$  arranged on perfect lattices. The two lattice types considered were the square (SQ, cf simple cubic in 3D) and  $\Lambda_1$  with lattice vectors  $(1.575a, 1.575a)$  and  $(-0.418a, 1.994a)$ , the densest packing configuration for superdisks with this shape parameter [49].

The relative interaction energies of these phases due to a force acting up to a certain range was estimated by computing the fraction of a particle perimeter in range of the surface of a neighbouring particle. This was done by placing 8000 points equally spaced along the perimeters of the superdisks in the lattice and counting what fraction of the points on the central particle are in range of a point on a neighbouring particle. The binary assignment of each point in this approximation is comparable to a square well potential extending perpendicularly to the surface with a certain range. Further details of this calculation may be found in figure S2.

### 3. Results and discussion

#### 3.1. Critical Casimir force driven assembly

The assembly of the colloidal cubes driven by critical Casimir forces was investigated in a quasi 2D system established in a 28.40 wt% lutidine–water mixture. When allowed to equilibrate at room temperature, the particles sedimented to the bottom of the capillary with thermal motion in height on the order of the gravitational length,  $l_g \sim D$ . Figure 2(a) shows a snapshot of the fluid of the charge stabilised silica cubes with area fraction  $\sim 24\%$ . Upon heating to a temperature just below  $T_{cx}$ , the small and transient clusters visible in figure 2(b) were

observed. Simultaneously, the particles were seen to lie flat on the glass such that they were confined to the horizontal  $xy$ -plane (for more details see figure S3). The approximate temperature at which particle clustering becomes observable is conventionally known as  $T_a$  [33], which in this case was  $33.16 \text{ }^\circ\text{C}$  ( $\Delta T = 0.46 \text{ }^\circ\text{C}$ ). Upon further heating to a temperature  $T_a < T < T_{cx}$ , stable and growing clusters formed (figure 2(c)).

Cluster formation confirms that the interparticle interactions changed from repulsive to attractive upon the increase in temperature. This change is due to the action of attractive critical Casimir forces between otherwise electrostatically repulsive particles [36]. The strength and range of these forces increase when temperature approaches  $T_{cx}$  [21], which explains the observation of increasingly stable clusters upon heating.

The crystalline arrangement of the particles in clusters up to  $\Delta T = 0.26 \text{ }^\circ\text{C}$  is visible in figure 2(c). Two lattice types were observed: square (SQ) and hexagonal, with the former accounting for the majority of particles. The latter type is assumed to be the distorted hexagonal  $\Lambda_1$ -lattice which has the densest packing for superdisks with  $m = 2.9$  [49]. The insets in figure 2 show the particle assignments to one or neither of these lattice types according to the procedure in section 2.3. The dominance of the SQ lattice (red dots) over the  $\Lambda_1$  (blue dots) is visible in the inset of panel (c). Both of these phases have previously been observed in systems of superballs with depletion interactions [30]. The observed structures will be discussed in more detail in section 3.3.

#### 3.2. Reversible control of interactions

When an attractive force is induced between particles with flat faces, it might be expected that the large area of interaction would induce strong enough attraction to irreversibly aggregate the particles. Such an event would prevent the study of dynamics and equilibrium structure of the system and limit its utility as a model attractive system, as well as reduce the degree of control over it. To determine the range of control

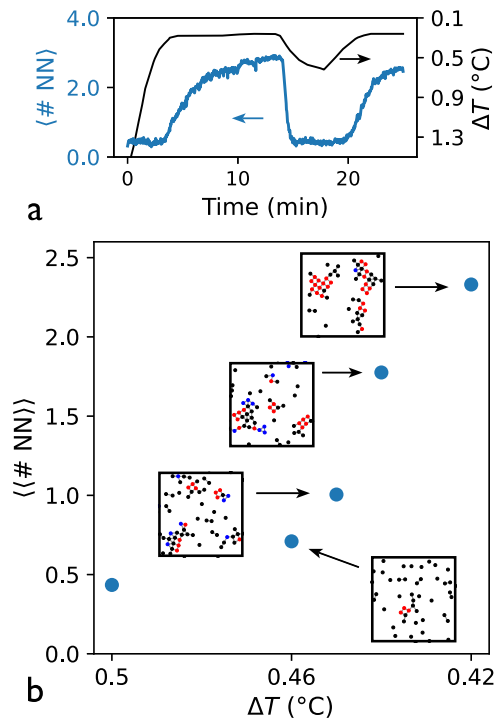


**Figure 3.** Particle clustering controlled by temperature. (a) The temperature of the system relative to separation (black line and right axis) and average number of neighbours for each particle (blue line, left axis) showing reversible clustering upon heating above  $\Delta T = 0.27$  °C and disassembly upon cooling below  $T_a$  at  $\Delta T = 0.46$  °C. The arrows indicate which vertical axis corresponds to each line. (b) Average equilibrated cluster size at different  $\Delta T$ . Histograms of the distributions can be found in figure S4. Insets show detected particle positions and lattice assignments of single CLSM snapshots (similar to insets figure 2).

the critical Casimir force offers over the assembly of the colloidal cubes, the temperature of the system was cycled close to  $T_{cx}$  (black line in figure 3(a)). To quantify the clustering in response to the temperature changes, the average number of neighbours assigned to each particle in each frame was determined,  $\langle \#NN \rangle$  (blue line in figure 3(a)). This quantity indicates the degree of clustering as it is minimised for free single particles in isotropic fluid and maximised with all particles in a single dense cluster.

The changes in  $\langle \#NN \rangle$  reveal that clustering of the particles started when the temperature was raised above  $T_a$ , where the attractive interactions become strong enough for aggregation. When the temperature was lowered below  $T_a$ , the system rapidly disassembled back to the fluid, while further heating induced assembly again. That the same clustering behaviour was observed in both heating cycles, confirms the full reversibility of the assembly mechanism for the colloidal cubes and the absence of any stability loss.

Figure 3(a) further shows that the assembly process is slow, while the disassembly of clusters occurs rapidly. The difference can be explained by the diffusion limitation of both processes. To partially decouple the time and temperature (i.e. kinetic and thermodynamic) effects, the system was held at constant temperature for 8 min during which it reached a quasi steady state. ‘Quasi’ here means that single particle adsorption/desorption from clusters had equilibrated, but true

equilibrium was not in general reached due to slow diffusion of large clusters.

Figure 3(b) shows the  $\langle \#NN \rangle$  averaged over 1 min (40 frames each containing  $\sim 500$  particles) in the steady state. The temperature range shown for the time-averaged measurements is chosen around the boundary of observable attraction. With an increase in temperature from  $\Delta T = 0.46$  °C to  $\Delta T = 0.42$  °C, the system changed from one with small transient clusters to one containing permanent clusters coexisting with adsorbing and desorbing single particles. The control over cluster size and the formation of stable clusters reveals that even for these cubic particles, which have large overlap in contact area, the critical Casimir force offers fine control over their assembly with interaction strengths on the order of the thermal energy.

While it would be insightful to continue these equilibrated measurements to smaller  $\Delta T$ , we observed particles sticking to the glass after spending a long time in the attractive regime. We believe that this unfortunate limitation may be overcome in future work by modifying the glass surface treatment. To avoid sticking in the current system and probe the behaviour at low  $\Delta T$ , fast ramping was used and the results of this are presented in the following section.

### 3.3. Effect of changing interparticle potential

To investigate the effect of changing the interparticle potential on structure, the whole  $\Delta T$  region between  $T_a$  and  $T_{cx}$  was explored. For this the temperature was raised rapidly ( $\sim 0.1$  °C  $\text{min}^{-1}$ ) from below  $T_a$  to above  $T_{cx}$  while imaging (for full sequence see supplementary movie 1). With increasing temperature, a structural transition from majority square to majority  $\Lambda_1$  symmetry was observed as shown in figure 4. Panels (a)–(c) show the transition observed in a single cluster during the temperature increase. At lower temperature,  $\Delta T = 0.14$  (figure 4(a)), this cluster showed predominantly square symmetry but transitioned almost fully to  $\Lambda_1$  symmetry when the temperature was increased to  $\Delta T = 0.06$  (figure 4(c)). Figure 4(b) at intermediate temperature gives an indication of the transition pathway, namely via sliding of whole rows of cubes. As the leftmost row slid downward, the cubes moved to the gaps in the adjacent row and thus switched to  $\Lambda_1$  symmetry. The result is that the cubes in the next row had environments with both square and hexagonal character and hence are not assigned to either lattice. After this first transition, all other rows also slid down, resulting in the  $\Lambda_1$  cluster in figure 4(c). For detailed analysis of the cluster see supplementary movie 2.

The fractions of particles in square and  $\Lambda_1$  environments of all  $\sim 600$  particles observed during the heating process are shown in figure 4(d). At  $\Delta T > 0.4$ , the assignment of each lattice symmetry is roughly equal. The lack of dominant square assignment at this temperature is attributed to the rapid heating preventing relaxation to square clusters, like those in figure 2(c). When the temperature was increased the proportion of  $\Lambda_1$  assignments grew rapidly at the expense of the square ones, showing that transitions such as that shown in figures 4(a)–(c) occurred not only in this cluster, but represent a more general phenomenon.

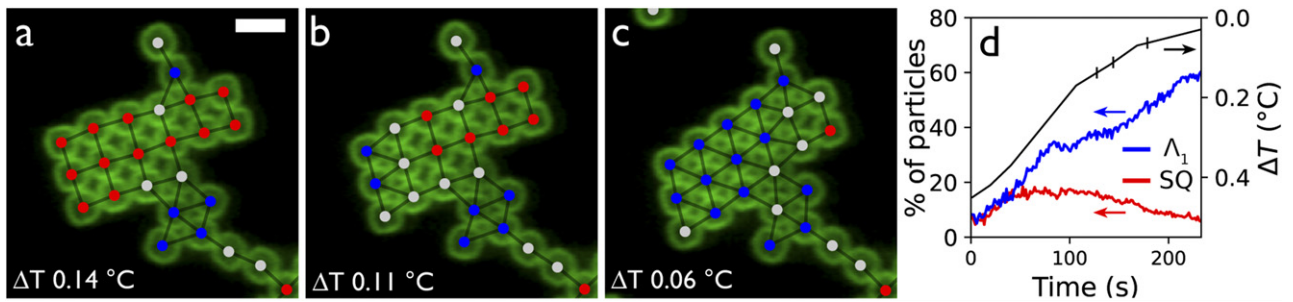


**Figure 4.** Structural transition. (a)–(c) CLSM snapshots with detected particle positions at different temperatures during a temperature ramp with ( $\sim 0.1^\circ\text{C min}^{-1}$ ) towards  $T_{\text{cx}}$  with assigned lattice environments: square (red),  $\Lambda_1$  (blue) and non-assigned (grey). The lines connecting particles indicate their NNs, which were used for computation of  $\psi_4$  and  $\psi_6$ . (d) Evolution of square (red line) and  $\Lambda_1$  (blue line) assigned particle environments with temperature for all 600 imaged particles, together with temperature profile (black line and right axis). The arrows indicate the vertical axis to which the data lines correspond. The vertical markers on the temperature line indicate the times of the snapshots in (a)–(c). Scale bar in (a) is  $2\ \mu\text{m}$ .

### 3.4. Structural transition

To understand the observed transition from square to  $\Lambda_1$  lattice in the superstructures of cubes, we take a closer look at the cube shape and the attractive critical Casimir interactions. For the hollow silica cubes it is well known that they possess a finite roundness of their corners and faces that makes their shape best approximated with that of a superball [8, 30, 43]. The cubic colloids employed here possess  $m = 2.9$ , indicating a very rounded cube, for which the predicted densest packings in 2D are the hexagonal-like  $\Lambda_0$ -lattice and rhombic  $\Lambda_1$ -lattice [49]. These two lattices achieve a higher packing density than the face-to-face arrangement of the square phase, due to an offset of the curved faces. Indeed, being a suboptimal packing, the square (or simple cubic) symmetry does not appear in systems of equilibrated repulsive superballs [43, 50]. However, a square superball phase has been observed with attractive depletion interactions in the studies of Rossi *et al* [8, 30]. In their work [30], the appearance of the square phase is attributed to the large overlap of exclusion zones with particles in face-to-face contact. In addition, in the same study a strikingly similar transition from square to  $\Lambda_1$  was observed upon increasing the depletant size. This was shown to be in agreement with predictions from excluded volume calculations and rationalised by the fact that smaller depletants can fit into the voids and exert an osmotic pressure which stabilises the square phase.

The strikingly similar transition from square to  $\Lambda_1$  is, however, induced differently in the system of Rossi *et al* and the current work, that is by increasing the depletant size [30] and by increasing the temperature towards  $T_{\text{cx}}$ , respectively. To understand what causes the transition, we have to address the question: What do these two studies have in common? Both observed structural changes correspond to an increase in the range of the effective attraction between the particles. In the case of depletion attraction larger depletants sizes lead to larger exclusion zones, while in the case of the critical Casimir force the range of the attractive force scales with the solvent correlation length which increases upon approaching  $T_{\text{cx}}$ . Therefore we hypothesise that the square

phase in both systems is stabilised by short range attractions and the higher density phase is favoured when the attraction range is increased. This is consistent with the depletion system [30] as well as the fact that for charged superballs interacting via short-range van der Waals attraction a face-to-face arrangement leads to the lowest energy state of two cubes [51].

To test our hypothesis that the changing range of the attractive force combined with the cubic shape is sufficient to stabilise one phase over the other, we calculate the effect of changing attraction range on surface interaction between superdisks. In line with the experiments, we examine particles with  $m = 2.9$  and approximate the interaction strength in the square and  $\Lambda_1$  phases. The strength of interaction of the central particle with its neighbours is determined by calculating the fraction of its perimeter that is in range of a neighbouring particle surface with the method described in section 2.4.

Figure 5(a) shows the sections of the particle surface which are in range of a neighbour in pink and those that are not in light blue. The pink regions all lengthen upon increasing the range from 10 to 50 nm. Figure 5(b) shows how much the surface contact increases in total for the two phases. The solid lines show that the square phase has the largest contact at short range but that for the  $\Lambda_1$  lattice the contact grows more rapidly with increasing range. This results in a crossover in fractional contact from square to  $\Lambda_1$  for a range above 31 nm. The dotted lines in figure 5(b) show the contributions of the different contact site types in the  $\Lambda_1$  lattice and these explain why the crossover occurs. The upper line shows the contribution of the four ‘face’ sites which have a similar behaviour to the square phase. The lower dashed line shows the contact of the ‘corner’ sites, that have a small contribution but nonetheless are completely absent in the square phase. This extra contact from the additional two neighbours in  $\Lambda_1$  leads to a greater contact area and once the interaction range is long enough their contribution becomes non-negligible.

Having predicted the crossover between the two phases to occur at 31 nm, the question remains: at what temperature



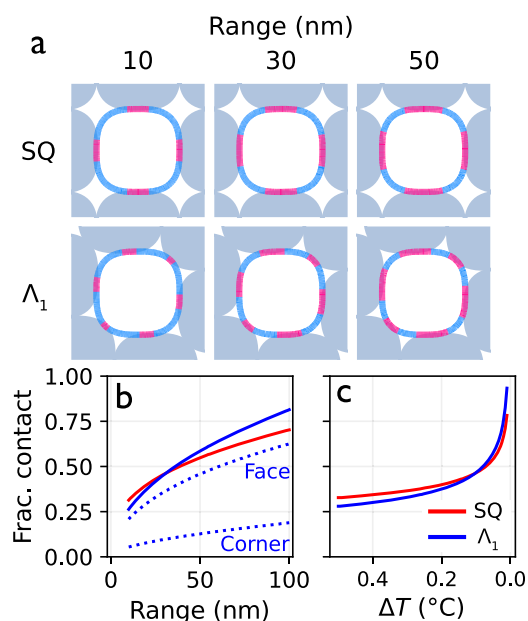


**Figure 5.** Influence of attraction range on interactions. (a) Calculation of cube surfaces that will interact based on surface-to-surface distance in a dense square lattice (top row) and  $\Lambda_1$  lattice (bottom row) for perfect superdisks with  $m = 2.9$  and an increasing range of the attractive force. The section of the particle's perimeter within range are labeled pink, while sections that are out of range are labeled blue. (b) Total fractions of the perimeter in range for the square phase (red line) that has greater contact at short range and  $\Lambda_1$  phase (blue) at longer range. The contact area in  $\Lambda_1$  is decomposed into the two corner and four face contributions (dotted lines), showing that the 'extra' corner contacts drives the transition from square to  $\Lambda_1$  with increasing range. (c) Evolution of fraction of cube surface in contact with temperature, based on the critical Casimir solvent correlation length  $\xi$ .

does the critical Casimir force reach this range? Computation of the interparticle potential resulting from this force is difficult, especially for anisotropic particles [52]. Therefore we approximate the range of the force as the solvent fluctuation correlation length,  $\xi$ , which is closely related to the range of the critical Casimir force [53]. The dependence of  $\xi$  on  $T$  was computed using the theory of [35] (values in figure S5). The computed  $\xi$  values were used as a range to calculate the fractional contact as a function of  $\Delta T$ . Figure 5(c) shows the results of the calculation and predicts the crossover to a preferred  $\Lambda_1$  phase at  $\Delta T = 0.1$  °C, which agrees well with the  $\Delta T$  where we observe a transition.

With the prediction of a change in the preferred phase at low  $\Delta T$ , our simple model suggests that the combination of the superball shape combined with the changing range of the critical Casimir force is the explanation for the observed transition. The fast ramp in the experiment of figure 4 means that an exact point of crossover could not be determined, but the experiment is in qualitative agreement with the model. To improve confidence in this explanation, more detailed experiments with longer equilibration times are required. Furthermore, the model uses a crude approximation of the force and does not account for the entropy of the phases, which may be significant and will require further investigations.

## 4. Conclusions

We have shown that the interactions between colloidal cubes can be finely controlled using the critical Casimir force. With the temperature as the single control variable, clustering was induced in quasi-2D by changing the interparticle potential from repulsive to attractive. This process was completely reversible, despite the flat particle faces being brought into close contact in the clusters.

The combination of cubic shape with an attractive interaction force of which the range and strength can be tuned by temperature, resulted in different superstructures. At temperatures very close to solvent phase separation, the densest packing  $\Lambda_1$  phase was found to form, while at lower temperature in the attractive regime, the simple square lattice was dominant. We propose that the less densely packing square phase is stabilised by very short range attractions at lower temperature and the crossover to the denser  $\Lambda_1$  phase occurs due to the increasing range of the force close to  $T_{cx}$  and the larger contribution of cube corners, due to their finite roundness. Our results shed new light onto the previously observed structural transitions in attractive superballs, and open up new routes to explore the self-assembly behaviour of cubic particles and other shape anisotropic particles in general.

## Acknowledgments

We thank Steffen Lootsma for preliminary analysis, Max Schelling for TEM imaging and Piet Swinkels for experimental assistance. We gratefully acknowledge Hannah Jonas, Peter Bolhuis and Piet Swinkels for fruitful discussions. JMM acknowledges financial support from the Netherlands Organization for Scientific Research (NWO) (016.Veni.192.119).

## Data availability statement

The data generated and/or analysed during the current study are not publicly available for legal/ethical reasons but are available from the corresponding author on reasonable request.

## ORCID iDs

Chris L Kennedy  <https://orcid.org/0000-0002-2942-4056>  
 Janne-Mieke Meijer  <https://orcid.org/0000-0002-5148-9948>

## References

- [1] Pusey P N and van Megen W 1986 *Nature* **320** 340–2
- [2] van der Kooij F M and Lekkerkerker H N W 1998 *J. Phys. Chem. B* **102** 7829–32
- [3] van der Kooij F M, Kassapidou K and Lekkerkerker H N W 2000 *Nature* **406** 868–71
- [4] Kuijk A, van Blaaderen A and Imhof A 2011 *J. Am. Chem. Soc.* **133** 2346–9

- [5] Hueckel T, Hocky G M and Sacanna S 2021 *Nat. Rev. Mater.* **6** 1053–69
- [6] Xia Y, Xiong Y, Lim B and Skrabalak S E 2008 *Angew. Chem., Int. Ed.* **48** 60–103
- [7] Li W, Palis H, Mérindol R, Majimel J, Ravaine S and Duguet E 2020 *Chem. Soc. Rev.* **49** 1955–76
- [8] Rossi L, Sacanna S, Irvine W T M, Chaikin P M, Pine D J and Philipse A P 2011 *Soft Matter* **7** 4139–42
- [9] Gong Z, Hueckel T, Yi G-R and Sacanna S 2017 *Nature* **550** 234–8
- [10] Boles M A and Talapin D V 2014 *J. Am. Chem. Soc.* **136** 5868–71
- [11] Vutukuri H R, Imhof A and van Blaaderen A 2014 *Angew. Chem., Int. Ed.* **53** 13830–4
- [12] Marin O *et al* 2019 *J. Colloid Interface Sci.* **538** 541–5
- [13] Damasceno P F, Engel M and Glotzer S C 2012 *Science* **337** 453–7
- [14] Dijkstra M 2014 *Entropy-Driven Phase Transitions in Colloids: From Spheres to Anisotropic Particles* (New York: Wiley) ch 2 pp 35–71
- [15] Li B, Wang F, Zhou D, Peng Y, Ni R and Han Y 2016 *Nature* **531** 485–8
- [16] Lekkerkerker H and Tuinier R 2011 *Colloids and the Depletion Interaction* (Springer)
- [17] Ruiz-Franco J and Zaccarelli E 2021 *Annu. Rev. Condens. Matter Phys.* **12** 51–70
- [18] Jones M R, Macfarlane R J, Lee B, Zhang J, Young K L, Senesi A J and Mirkin C A 2010 *Nat. Mater.* **9** 913–7
- [19] Wang Y, Wang Y, Zheng X, Ducrot É, Yodh J S, Weck M and Pine D J 2015 *Nat. Commun.* **6** 7253
- [20] Quan Z *et al* 2014 *J. Am. Chem. Soc.* **136** 1352–9
- [21] Hertlein C, Helden L, Gambassi A, Dietrich S and Bechinger C 2008 *Nature* **451** 172–5
- [22] Lin H, Lee S, Sun L, Spellings M, Engel M, Glotzer S C and Mirkin C A 2017 *Science* **355** 931–5
- [23] Brunner J, Baburin I A, Sturm S, Kvashnina K, Rossberg A, Pietsch T, Andreev S, Rosseeva E S n and Cölfen H 2017 *Adv. Mater. Interfaces* **4** 1600431
- [24] Disch S *et al* 2013 *Nanoscale* **5** 3969–75
- [25] Petukhov A V, Tuinier R and Vroege G J 2017 *Curr. Opin. Colloid Interface Sci.* **30** 54–61
- [26] Kleshchanok D, Meijer J-M, Petukhov A V, Portale G and Lekkerkerker H N W 2012 *Soft Matter* **8** 191–7
- [27] Lefterink op Reinink A B G M, Belli S, van Roij R, Dijkstra M, Petukhov A V and Vroege G J 2014 *Soft Matter* **10** 446–56
- [28] Badaire S, Cottin-Bizonne C, Woody J W, Yang A and Stroock A D 2007 *J. Am. Chem. Soc.* **129** 40–1
- [29] Hsiao L C, Schultz B A, Glaser J, Engel M, Szakasits M E, Glotzer S C and Solomon M J 2015 *Nat. Commun.* **6** 8507
- [30] Rossi L, Soni V, Ashton D J, Pine D J, Philipse A P, Chaikin P M, Dijkstra M, Sacanna S and Irvine W T M 2015 *Proc. Natl Acad. Sci. USA* **112** 5286–90
- [31] García Á G, Opdam J and Tuinier R 2018 *Eur. Phys. J. E* **41** 110
- [32] Dekker F, García Á G, Philipse A P and Tuinier R 2020 *Eur. Phys. J. E* **43** 38
- [33] Bonn D, Otwinowski J, Sacanna S, Guo H, Wegdam G and Schall P 2009 *Phys. Rev. Lett.* **103** 156101
- [34] Gambassi A, Maciołek A, Hertlein C, Nellen U, Helden L, Bechinger C and Dietrich S 2009 *Phys. Rev. E* **80** 061143
- [35] Stuij S G, Labbé-Laurent M, Kodger T E, Maciołek A and Schall P 2017 *Soft Matter* **13** 5233–49
- [36] Maciołek A and Dietrich S 2018 *Rev. Mod. Phys.* **90** 045001
- [37] Nguyen V D, Faber S, Hu Z, Wegdam G H and Schall P 2013 *Nat. Commun.* **4** 1584
- [38] Edison J R, Tasios N, Belli S, Evans R, van Roij R and Dijkstra M 2015 *Phys. Rev. Lett.* **114** 038301
- [39] Yu C, Zhang J and Granick S 2014 *Angew. Chem., Int. Ed.* **53** 4364–7
- [40] Stuij S G, Jonas H J, Gong Z, Sacanna S, Kodger T E, Bolhuis P G and Schall P 2021 *Soft Matter* **17** 8291–9
- [41] Swinkels P J M *et al* 2021 *Nat. Commun.* **12** 2810
- [42] Marino E, Vasilyev O A, Kluff B B, Stroink M J B, Kondrat S and Schall P 2021 *Nanoscale Horiz.* **6** 751–8
- [43] Meijer J M, Pal A, Ouhajji S, Lekkerkerker H N W, Philipse A P and Petukhov A V 2017 *Nat. Commun.* **8** 14352
- [44] Grattoni C A, Dawe R A, Seah C Y and Gray J D 1993 *J. Chem. Eng. Data* **38** 516–9
- [45] Mirzaev S Z, Behrends R, Heimburg T, Haller J and Kaatz U 2006 *J. Chem. Phys.* **124** 144517
- [46] White K A, Schofield A B, Wormald P, Tavecchi J W, Binks B P and Clegg P S 2011 *J. Colloid Interface Sci.* **359** 126–35
- [47] Stuij S G 2020 *Colloidal design: building, bending and breaking* *PhD Thesis* University of Amsterdam
- [48] Allan D B, Caswell T, Keim N C and van der Wel C M 2019 *Trackpy v0.4.2*
- [49] Jiao Y, Stillinger F H and Torquato S 2008 *Phys. Rev. Lett.* **100** 245504
- [50] Ni R, Gantapara A P, de Graaf J, van Roij R and Dijkstra M 2012 *Soft Matter* **8** 8826
- [51] Rosenberg M, Dekker F, Donaldson J G, Philipse A P and Kantorovich S S 2020 *Soft Matter* **16** 4451–61
- [52] Jonas H J, Stuij S G, Schall P and Bolhuis P G 2021 *J. Chem. Phys.* **155** 034902
- [53] Krech M 1999 *J. Phys.: Condens. Matter.* **11** R391–412